

ARTICLE

DOI: 10.1038/s41467-018-06294-y

OPEN

# Efficient photocatalytic hydrogen evolution with ligand engineered all-inorganic InP and InP/ZnS colloidal quantum dots

Shan Yu<sup>1,2</sup>, Xiang-Bing Fan<sup>3</sup>, Xian Wang<sup>4</sup>, Jingguo Li<sup>2</sup>, Qian Zhang<sup>1,2</sup>, Andong Xia<sup>4</sup>, Shiqian Wei<sup>1</sup>, Li-Zhu Wu<sup>3</sup>, Ying Zhou<sup>1</sup> & Greta R. Patzke<sup>2</sup>

Photocatalytic hydrogen evolution is a promising technique for the direct conversion of solar energy into chemical fuels. Colloidal quantum dots with tunable band gap and versatile surface properties remain among the most prominent targets in photocatalysis despite their frequent toxicity, which is detrimental for environmentally friendly technological implementations. In the present work, all-inorganic sulfide-capped InP and InP/ZnS quantum dots are introduced as competitive and far less toxic alternatives for photocatalytic hydrogen evolution in aqueous solution, reaching turnover numbers up to 128,000 based on quantum dots with a maximum internal quantum yield of 31%. In addition to the favorable band gap of InP quantum dots, in-depth studies show that the high efficiency also arises from successful ligand engineering with sulfide ions. Due to their small size and outstanding hole capture properties, sulfide ions effectively extract holes from quantum dots for exciton separation and decrease the physical and electrical barriers for charge transfer.

<sup>1</sup>School of Materials Science and Engineering, Southwest Petroleum University, No. 8, Xindu Road, Xindu District, Chengdu 610500, China. <sup>2</sup>Department of Chemistry, University of Zurich, Winterthurerstrasse 190, CH-8057 Zurich, Switzerland. <sup>3</sup>Key Laboratory of Photochemical Conversion and Optoelectronic Materials, Technical Institute of Physics and Chemistry, Chinese Academy of Sciences, Beijing 100190, China. <sup>4</sup>Beijing National Laboratory for Molecular Sciences, Key Laboratory of Photochemistry, Institute of Chemistry, Chinese Academy of Sciences, Beijing 100190, China. These authors contributed equally: Shan Yu, Xiang-Bing Fan. Correspondence and requests for materials should be addressed to L.-Z.W. (email: [lzwu@mail.ipc.ac.cn](mailto:lzwu@mail.ipc.ac.cn)) or to Y.Z. (email: [yzhou@swpu.edu.cn](mailto:yzhou@swpu.edu.cn)) or to G.R.P. (email: [greta.patzke@chem.uzh.ch](mailto:greta.patzke@chem.uzh.ch))

Conversion of solar energy into storable hydrogen fuel through water splitting is one of the most sustainable solutions to meet the increasing worldwide energy demands<sup>1,2</sup>. Among the wide spectrum of photosensitizer types that has emerged over the past years<sup>3–8</sup>, colloidal quantum dots (QDs) stand out through combining molecular versatility with the efficient light harvesting properties of semiconductors<sup>9,10</sup>, and facile charge carrier transport through interfaces<sup>10,11</sup>. Photocatalytic processes with semiconductor nanomaterials and QDs<sup>12,13</sup>, such as CdS, do not only provide most direct low-tech access to clean hydrogen, but also permit fundamentally new insight into the photophysics of hydrogen production<sup>14</sup>. CdS/CdO<sub>x</sub> QDs furthermore open up new avenues for solar photo-reforming of lignocellulose biomass to hydrogen<sup>15</sup>. To date, Cd-chalcogen II–IV QDs remain the most efficient QD types in photocatalytic systems<sup>15–20</sup>. However, the toxicity of Cd severely limits their large-scale application options, not only in photocatalytic water splitting, but also in other urgent global challenges, such as water disinfection<sup>21</sup> and the elimination of multidrug-resistant bacteria<sup>22</sup> with photoexcited QDs. This current need for efficient non-toxic QDs has brought forward complex engineering approaches towards multinary I–III–VI<sub>2</sub> and I<sub>2</sub>–II–IV–VI<sub>4</sub> nanoscale semiconductors<sup>23</sup>.

InP QDs are an attractive alternative target for direct solar-to-fuel conversion. Furthermore, InP is well suited for environmental and biological applications<sup>24</sup>, and the notably lower toxicity of InP/ZnS QDs compared to CdSe/ZnS QDs has recently been demonstrated both in vitro and in vivo<sup>25</sup>. Surprisingly, however, InP QDs have rarely been studied for their artificial photosynthesis properties, although InP nanomaterials were used in breakthrough photoelectrode and solar cell studies<sup>26,27</sup>. In comparison to the most widely investigated CdSe QDs, InP has a smaller bulk band gap (1.35 eV vs 1.76 eV) and larger Bohr exciton radius (9.6 nm vs 4.6 nm), which widens its corresponding absorption and emission range. In addition, InP displays a more evident extent of covalent bonding than CdSe, leading to higher delocalization of wavefunctions and weaker attraction between electrons and holes, as well as weaker phonon coupling<sup>24</sup>.

Here we show the potential of InP QDs as hydrogen evolution photosensitizers. Inspired by recent synthetic developments<sup>28</sup>, we access a series of InP and InP/ZnS QDs using economic and safe (dialkylamino)phosphines as phosphorus source. Modification of the as prepared QDs with inorganic sulfide (S<sup>2–</sup>) ions<sup>29,30</sup> furthermore brings forward progress in ligand engineering of QDs, as a key area in solar energy conversion<sup>31</sup>. These sulfide ions not only endow QDs with good water solubility, but also with remarkable activity in photocatalytic processes<sup>32</sup>. We demonstrate the important role of S<sup>2–</sup> ligands for photocatalytic hydrogen evolution by comparing different organic and inorganic ligand types. S<sup>2–</sup> ligands not only effectively facilitate the extraction of photogenerated holes from the QDs to the surface ligands, but also decrease the charge transfer barriers between QDs and their surrounding acceptors, thus notably enhancing photocatalytic hydrogen evolution.

## Results

**Synthesis and characterization.** InP and InP/ZnS colloidal QDs were synthesized based on a modified literature protocol (see Supplementary Fig. 1 for photographs)<sup>28,33</sup>. First, the size of the QDs was adjusted by tuning the ratio of ZnCl<sub>2</sub> to ZnI<sub>2</sub>, instead of introducing of different indium halides. Furthermore, the growth temperature for ZnS was directly held constant at a higher value prior to the addition of sulfur (cf. Methods, Supplementary Method 1 and Supplementary Note 1 for further information).

The characteristic absorption peak of the QDs undergoes a blue shift from 570 nm to 435 nm upon increasing the ratio of ZnI<sub>2</sub> to ZnCl<sub>2</sub> in the system (Fig. 1a). Likewise, the emission peak of InP/ZnS QDs is shifted from 605 nm to 515 nm (Fig. 1b). The typical emission spectra of the as-synthesized InP/ZnS QDs exhibit FWHM (full width at half maximum) values around 60 nm, close to the reported optimal results<sup>33–35</sup>. While coating of InP QDs with ZnS barely changes the absorption spectrum of the original InP QDs, it leads to a significant improvement of the photoluminescence quantum yield (PLQY) of the system from 1.0 to 46% with increasing growth time of the capping layer (Supplementary Fig. 2). This confirms that the growth of ZnS on QDs efficiently passivates their surfaces<sup>36</sup>.

Ligand exchange was then carried out to replace the original long-chain organic ligands (oleylamine, OLA) on the surface of the QDs (referred to QDs-OLA) with inorganic S<sup>2–</sup> (referred to QDs-S; cf. Methods for details)<sup>30</sup>. The success of this process is evident from the efficient phase transfer of the treated QDs from hexane to *N*-Methylformamide (NMF) (inset of Fig. 1c). These S<sup>2–</sup> capped QDs could be well dissolved in water by further precipitation and redispersion, in line with their sufficiently negative zeta potential (Supplementary Fig. 3). The excitonic features in the absorption spectra remain constant after ligand exchange, implying that the size changes of the QDs are negligible after sulfide capping (Fig. 1c and Supplementary Fig. 4)<sup>30,37</sup>. Nevertheless, the PLQY of InP/ZnS QDs after ligand exchange dropped drastically (Fig. 1c) due to the increased amount of surface traps and nonradiative relaxation processes<sup>38,39</sup>. Efficient ligand exchange is furthermore evident from the almost complete disappearance of the ligand C–H stretching FT-IR bands at 2855 and 2924 cm<sup>–1</sup> (Fig. 1d)<sup>29,30</sup>. In addition, thermogravimetric analysis (TGA) of S<sup>2–</sup> capped QDs shows no obvious weight loss between 100 and 500 °C in contrast to ligand loss of OLA capped QDs (Supplementary Fig. 5), thus providing further evidence for the removal of most organic ligands<sup>29,37</sup>.

TEM and HRTEM images indicate a typical narrow size distribution of the InP QDs (525 nm) with an average size around 2.7 nm, which is close to literature data<sup>28</sup>. After growth of ZnS for 15 min, the size of QDs changed slightly (Supplementary Figs. 6 and 8). After ligand exchange, the shape and size of InP and InP/ZnS QDs did not change obviously (Supplementary Figs. 7 and 8), although a slight degree of aggregation took place due to the less repulsive effect of inorganic sulfide ions compared to long-chain organic molecules. Due to the very thin ZnS layer and the small size of QDs, the direct assignment of ZnS based on lattice planes or EDS elemental mapping is difficult. However, a less crystalline zone outside the InP core in the aberration-corrected STEM image (Supplementary Fig. 9) may arise from the surface modification of QDs with such a thin ZnS layer<sup>40</sup>. Powder X-ray diffraction (PXRD) data (Supplementary Fig. 10) confirm that the zinc blende structure of the QDs is maintained during both ZnS growth and ligand exchange processes, accompanied by a peak shift to higher angles from InP QDs to InP/ZnS QDs<sup>28,35</sup>. Elemental analyses by inductively coupled plasma optical emission spectrometry (ICP-OES, Supplementary Table 1) and energy-dispersive X-ray spectroscopy (SEM-EDS, Supplementary Table 2) both show that ZnS growth on InP QDs within 15 min is slow under the applied synthetic conditions, according to the low Zn/In atomic ratio in the QDs. Generally speaking, the notable lattice mismatch (7.7%) of ZnS and InP renders the growth of thick ZnS layers difficult<sup>36</sup>. Although ZnS layers obtained from longer reaction times would improve the PLQY of QDs (Supplementary Fig. 2b)<sup>28</sup>, it may not be an optimal choice for photocatalysis (see below). In addition, the sulfur content in the composites after ligand exchange increased obviously, which is in line with the above analysis.

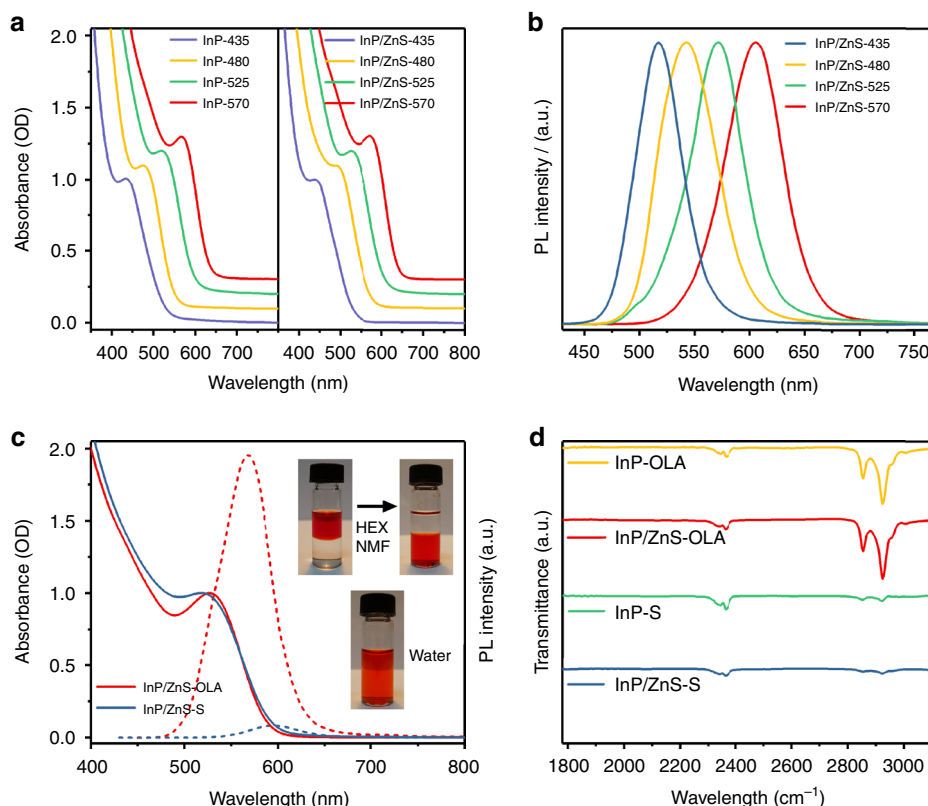


**Fig. 1** Spectroscopic characterization of InP and InP/ZnS QDs. **a** Absorption spectra of different InP and InP/ZnS (15 min) QDs in hexane. **b** PL spectra of different InP/ZnS (15 min) QDs in hexane. **c** Absorption spectra and PL spectra before and after ligand exchange for InP/ZnS QDs (525 nm, 15 min) in hexane and water (the absorbance of the two QD types was adjusted to the same value at the excitation wavelength to enable PL comparison). **d** FT-IR spectra of QDs before and after ligand exchange

**Photocatalytic hydrogen evolution.** After the concentration of the colloidal solution was determined (cf. Supplementary Method 2), InP-S and InP/ZnS-S QDs were tested for hydrogen evolution in the presence of ascorbic acid ( $H_2A$ ) as electron donor and  $Ni^{2+}$  as proton reduction catalyst, along the lines of the reported assays for Cd-based QDs<sup>17,41</sup>. Control experiments show that light, photoabsorber QDs, the electron donor  $H_2A$ , and the  $Ni^{2+}$  catalyst are all indispensable for efficient hydrogen evolution (Fig. 2a), and the optimal concentration of  $Ni^{2+}$  and  $H_2A$  as well as the optimal pH for the present system were studied (Supplementary Fig. 11). Moreover, we compared the photocatalytic performance with pristine InP-S QDs (525 nm) with two conventional CdSe-S QD batches from different protocols (with similar absorption peak, size, and ligand exchange procedures) under analogous conditions (see Supplementary Method 3). The results show that the hydrogen generation efficiency of InP QDs is even higher than that of CdSe QDs (Fig. 2b). This demonstrates that InP-based QDs bear a high potential for photocatalytic hydrogen evolution with environmentally friendly materials. Furthermore, the overall photocatalytic hydrogen evolution efficiency was enhanced after the growth of ZnS layers on InP QDs (Supplementary Fig. 12). In particular, InP/ZnS QDs with a ZnS growth time of 15 min (with a thin ZnS layer, see results above) outperform the other samples. As ZnS has a higher conduction band and a lower valence band, a type I heterostructure is formed between InP and ZnS. Therefore, electrons and holes tend to localize in InP. Although ZnS can decrease the concentration of some intrinsic surface defects, extraction of the photogenerated charges by  $Ni^{2+}$  and  $H_2A$  would be less efficient in case of a thick ZnS layer<sup>42</sup>, which is in sharp contrast to the requirements for high PLQY. Moreover, hydrogen evolution was

evaluated for InP and InP/ZnS QDs with different excitonic absorption peaks under illumination with an AM 1.5 solar simulator (Fig. 2c), and all of them exhibited good performance. This may result from their optimal band gap settings, which ensure both efficient absorption of the incident light from the solar simulator and the sufficient driving force for photogenerated charge transfer and subsequent reactions.

Under optimal conditions, photocatalytic hydrogen evolution was performed with different light sources (Supplementary Fig. 13). The hydrogen generation rate for the system reaches  $45 \text{ mmol h}^{-1} \text{ g}^{-1}$  within 64.5 h (see Supplementary Fig. 13a and Supplementary Method 4) with a LED light source, and the TON value is as high as 128,000 based on InP/ZnS-S QDs (and 5900 normalized to Ni centers). The apparent quantum yield (AQY) of the system correlates well with the absorption spectra of InP/ZnS QDs, and the internal quantum yield (IQY) reaches 31% at 525 nm (Supplementary Method 5, Supplementary Table 3 and Supplementary Fig. 14). When using an AM 1.5 solar simulator as an alternative light source, the TON and hydrogen evolution rate within 20 h are 61,500 and  $70 \text{ mmol h}^{-1} \text{ g}^{-1}$ , respectively (Supplementary Fig. 13b). Online photocatalytic hydrogen evolution tests show that InP/ZnS-S QD systems display long-term activity over 100 h (Fig. 2d). PXRD patterns further confirm that the diffraction peaks of QDs are still distinguishable after evolution of 0.65 mmol  $H_2$  (Supplementary Fig. 15). The decline of the hydrogen evolution rate after long time irradiation may be caused by the accumulation of the oxidation product dehydroascorbic acid (DHA)<sup>43</sup>, as well as by partial degradation of the QDs. However, the total amount of  $H_2$  production is satisfactory and competitive in all of the investigated reaction conditions. The above results in

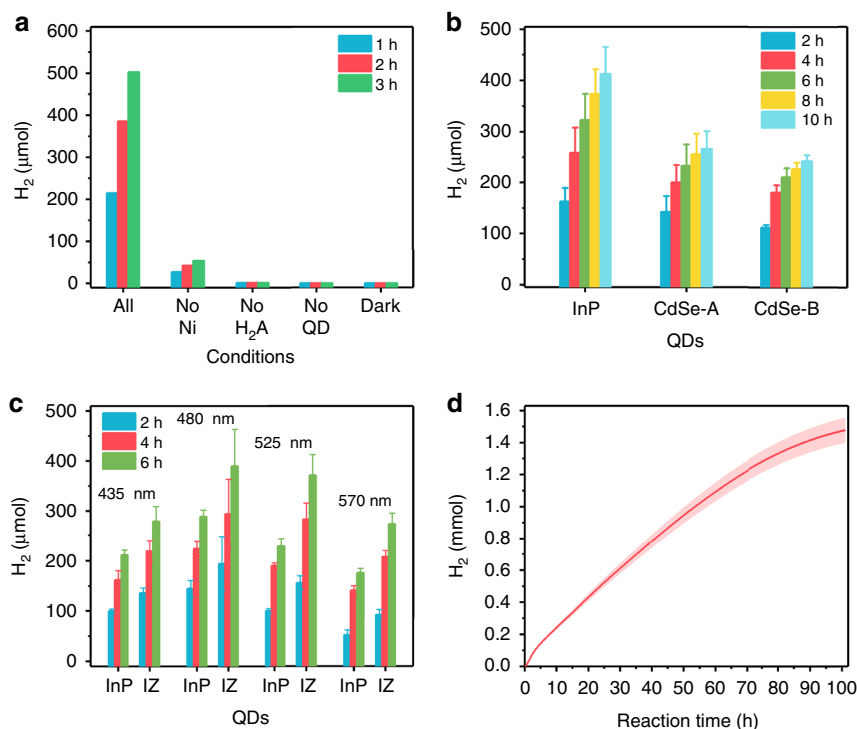


**Fig. 2** Photocatalytic hydrogen evolution experiments. **a** Amount of hydrogen evolved from reference systems without  $\text{Ni}^{2+}$ ,  $\text{H}_2\text{A}$ , QDs or light illumination, respectively. **b** Comparison of hydrogen evolution results with InP-S QDs (525 nm) and two types of CdSe-S QDs (~525 nm). **c** Hydrogen evolution with InP-S QDs and InP/ZnS QDs (abbreviated as IZ) with different excitonic absorption peaks. **d** Long time hydrogen evolution of InP/ZnS QDs (shadowed area: error range). Conditions: **a** 1.6  $\mu\text{M}$  InP/ZnS QDs, **b** 1.6  $\mu\text{M}$  InP-S QDs (525 nm) and CdSe-S QDs with the same absorbance at 525 nm or **c** 2  $\mu\text{mol}$  (of molecular concentration) QDs with different absorption peak, with 0.035 mM  $\text{Ni}^{2+}$  in 6 mL of 0.2 M  $\text{H}_2\text{A}$  (pH 4.5) were illuminated with **a, b** LED light source (525 nm,  $4 \times 1$  W) and **c** AM 1.5 simulator light; **d** 1.9  $\mu\text{M}$  QDs (525 nm, 15 min) and 0.042 mM  $\text{Ni}^{2+}$  in 10 mL of 0.2 M  $\text{H}_2\text{A}$  (pH 4.5) with LED light source (453 nm, 0.23 W). Error bars were estimated based on the standard deviation according to two or more independent experiments

their entirety clearly highlight  $\text{S}^{2-}$  capped InP and InP/ZnS QDs as a promising photosensitizer type.

**Photophysical study of the system.** To study the mechanisms behind the photocatalytic process, the thermodynamic properties of InP/ZnS QDs were first evaluated. The conduction and valence band edge positions of InP/ZnS QDs were determined as  $-0.92$  V and  $1.35$  V (vs NHE) through cyclic voltammetry (CV) measurements (Supplementary Fig. 16)<sup>44</sup>, in line with other reports<sup>26</sup>. Given the standard redox potentials of  $\text{Ni}^{2+}/\text{Ni}$  ( $-0.25$  V vs NHE) and  $\text{H}_2\text{A}/\text{DHA}$  ( $0.36$  V vs NHE)<sup>41,45</sup>, electron transfer from QDs to  $\text{Ni}^{2+}$  and hole transfer from QDs to  $\text{H}_2\text{A}$  thus appears feasible. DHA hydrate is the main oxidation product of  $\text{H}_2\text{A}$  after photocatalysis, which was verified through  $^{13}\text{C}$  NMR spectroscopy (Supplementary Fig. 17). However, the formation of metallic Ni was not detected by EPR spectroscopy of the present system after illumination (Supplementary Fig. 18), in line with some other reports<sup>17,46</sup>. In addition, no significant absorption changes were observed and the zeta potential of the system remained sufficiently negative at pH 4.5 (cf. Supplementary Fig. 19, Supplementary Note 2, and Supplementary Table 4). This indicates that the majority of the  $\text{S}^{2-}$  ligands on the QDs are retained under the photocatalytic conditions.

Time-resolved spectroscopy was then performed to obtain direct insight into the photophysical behavior of charge carriers. Femtosecond transient absorption (fs-TA) experiments were firstly conducted using a home-built femtosecond broadband pump-probe setup with time resolution around 100 fs as described previously in detail<sup>47</sup>. Concentrations of samples were adjusted to an absorbance of 0.3 OD at a pumping wavelength of

480 nm in 1 mm pathlength quartz cuvettes, and continuous stirring was performed during the test to alleviate photodegradation. The TA spectra (Fig. 3a, b) display two prominent features, namely a typical excitation bleaching (XB) and a featureless broad photoinduced absorption (PA). The XB signal is usually attributed to the state filling of the 1S electron level in the conduction band, as state filling of the 1S hole level is often negligible due to a higher density and degeneracy of the hole levels in QDs<sup>48,49</sup>. In contrast, both electrons and holes can be responsible for the PA signal, and it may vary with different QDs and surface states<sup>49,50</sup>. We here analyzed the origin of PA in the present system with respect to two aspects. One is the different decay behavior for the kinetics of XB and PA (Supplementary Fig. 20). This means that the species contributing to PA differs from that responsible for XB<sup>50</sup>. The other strategy is the analysis of the kinetic changes after  $\text{H}_2\text{A}$  and  $\text{Ni}^{2+}$  were introduced (Fig. 3d)<sup>49,51</sup>. When the electron donor  $\text{H}_2\text{A}$  is added, the decay of PA becomes faster, while no obvious changes occur after addition of  $\text{Ni}^{2+}$ . Therefore, we attribute the PA signals mostly to the holes in InP/ZnS QDs.

Based on this analysis, we further compared the kinetics for the XB (Supplementary Fig. 21a) and PA (Fig. 3c) signals of both InP/ZnS-OLA QDs and InP/ZnS-S QDs, respectively. For InP/ZnS-OLA QDs, the decay of TA signal is slow, indicating that the trap state within the QDs is suppressed, in line with their bright luminescence. After ligand exchange of OLA by  $\text{S}^{2-}$ , both XB and PA decay become faster. Usually,  $\text{S}^{2-}$  ligands can act as hole traps above the valence band<sup>38,52</sup>. Although the hole transfer to  $\text{S}^{2-}$  seemingly should not affect the kinetics of XB, the faster recovery of XB is not surprising (Supplementary Fig. 21a), given that there are numerous works reporting that the hole transfer



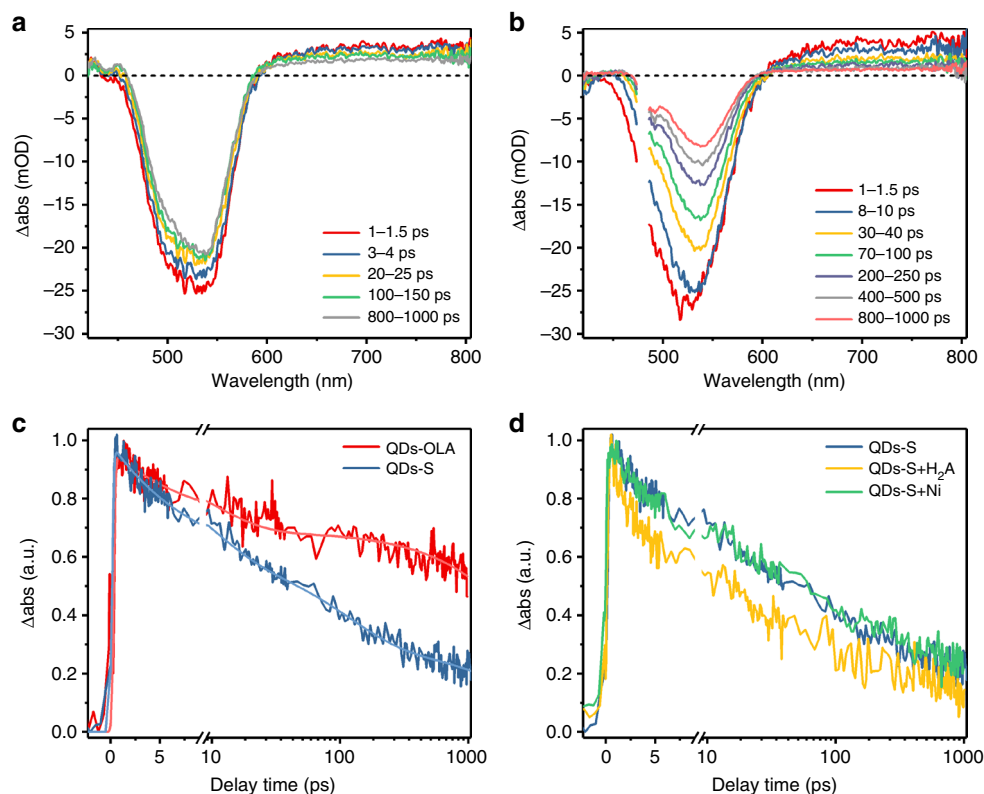


**Fig. 3** fs-TA spectra of InP/ZnS QDs (525 nm, 15 min). **a** TA spectra of InP/ZnS-OLA QDs; **b** TA spectra of InP/ZnS-S QDs at indicated delay time windows. **c** TA kinetics at 725 nm (average from 700 nm to 750 nm) for the PA signal and the corresponding fitting curve of InP/ZnS-OLA and InP/ZnS-S QDs. **d** TA kinetics at 725 nm (average from 700 nm to 750 nm) for the PA signal of InP/ZnS-S QDs with and without introduction of H<sub>2</sub>A or Ni<sup>2+</sup> into the solution. Conditions: pump pulses wavelength: 480 nm

process indeed leads to a faster decay of XB, which is still subject to discussions<sup>53–55</sup>. In contrast, the faster decay of the PA signal for holes in InP/ZnS-S QDs can be clearly explained with the hole transfer process (Fig. 3c). Other than OLA, the S<sup>2–</sup> ligands on the surface accept photogenerated holes from QDs, thus providing an additional pathway for hole extinction, which accelerates the disappearance of the hole related transient PA signal. Fitting of PA signal kinetics clearly illustrates that an additional decay process with a timescale around 110 ps appears for InP/ZnS-S QDs in comparison to InP/ZnS-OLA (Supplementary Table 5), which is consistent with the hole transfer process from QDs to S<sup>2–</sup> ligands.

Moreover, comparison of the kinetic decay of InP/ZnS-S QDs in the presence/absence of Ni<sup>2+</sup> or H<sub>2</sub>A demonstrates that charge transfer proceeds on the ps scale in the system. On the one hand, hole transfer is evident from the faster decay of the PA signal after the introduction of H<sub>2</sub>A into the solution (Fig. 3d); and on the other hand, electron transfer from QDs to Ni<sup>2+</sup> is observable as well from the faster recovery of the XB electron signal after the addition of Ni<sup>2+</sup> catalyst (Supplementary Fig. 21b)<sup>49,56</sup>.

Due to the limited timescale of the fs-TA experiment (up to 1 ns), further information about the charge transfer processes on the nanosecond scale was obtained from steady-state and time-resolved emission spectra of InP/ZnS-S QDs. The emission of the QDs was quenched notably after introduction of small amounts of Ni<sup>2+</sup> and H<sub>2</sub>A into the system, and this effect increased gradually with higher amounts (Fig. 4a, b). The kinetic emission decay of the QDs became faster as well, in line with the decrease of emission intensity (Fig. 4c, d). Fitting results show that the average lifetime of InP/ZnS QDs dropped from 37.0 ns to 17.7 ns and from 38.2 ns to 2.52 ns with Ni<sup>2+</sup> and H<sub>2</sub>A concentrations of 0.04 mM and 3 mM, respectively (see Supplementary Tables 6

and 7 and Supplementary Method 6). This points to a calculated electron transfer rate from QDs to Ni<sup>2+</sup> of  $7.64 \times 10^8 \text{ s}^{-1} \text{ mM}^{-1}$  and a hole transfer rate from QDs to H<sub>2</sub>A of  $1.25 \times 10^8 \text{ s}^{-1} \text{ mM}^{-1}$  (inset of Fig. 4c, d).

**Significance of sulfide capping.** The above analysis indicates that the surface S<sup>2–</sup> ligands influence the photophysical processes of QDs, which may also contribute to the high hydrogen evolution performance of the present system. We thus further explored the role of surface sulfide ligands beyond their endowing QDs with water solubility. To that end, we systematically compared InP/ZnS-S QDs to a series of QDs capped with other ligands with respect to their respective activity in photocatalytic hydrogen evolution. The ligands were selected with respect to two criteria. First the ligand exchange process should be easy and efficient, and secondly the ligands should stabilize InP and InP/ZnS QDs as colloids in solution.

Usually, colloidal QDs synthesized in organic phases are capped with oil-soluble long alkyl chains (OLA in the present case), and the conventional ligands used to transfer QDs from nonpolar solvents to water are organic thiols. We thus prepared InP/ZnS QDs capped with 3-mercaptopropionic acid (MPA) and 11-mercaptoundecanoic acid (MUA) by similar ligand exchange methods (named as InP/ZnS-MPA and InP/ZnS-MUA QDs, details in Supplementary Method 7), which are two widely used organic thiols for ligand exchange. Interestingly, the hydrogen evolution efficiency with these two QD types is considerably below that of InP/ZnS-S QDs (Fig. 5a). Similar phenomena have been observed in field effect transistors and in solar cells based on QDs with inorganic ligands over the past years<sup>30,31,57,58</sup>. Recent work also shows the inhibitory effect of thiol ligands on CdS QDs

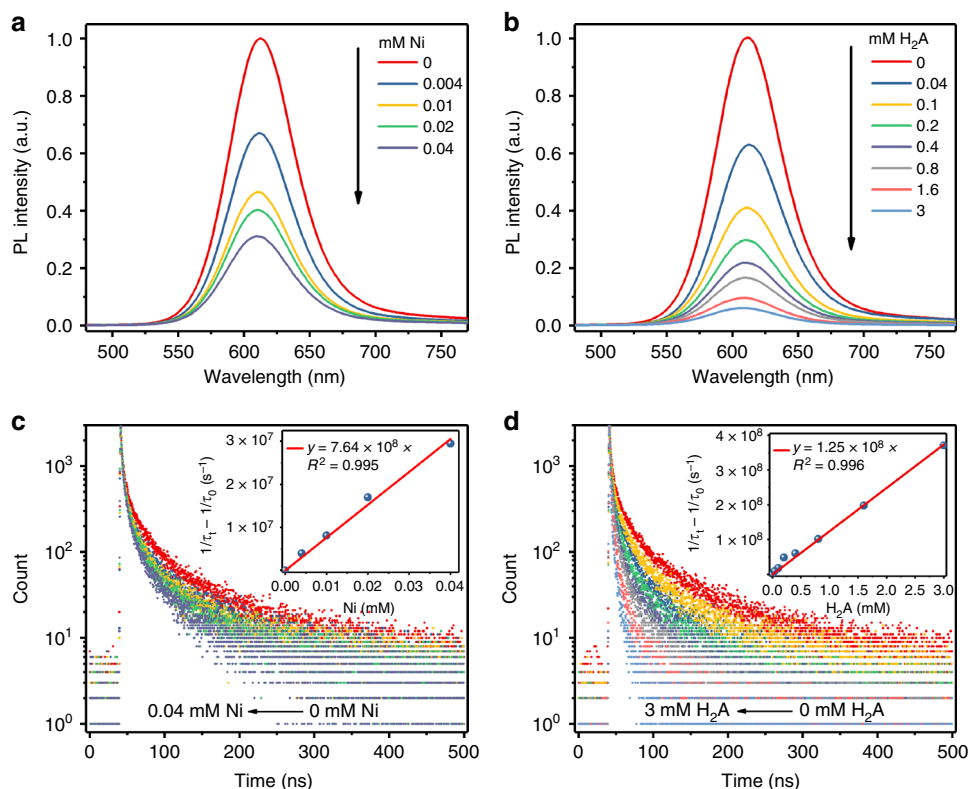


**Fig. 4** Steady state and time-resolved photoluminescence quenching experiment of InP/ZnS-S QDs (525 nm, 15 min). **a, b** Static photoluminescence quenching for InP/ZnS-S QDs in water after addition of different amounts of  $\text{Ni}^{2+}$  and  $\text{H}_2\text{A}$  respectively; the inset shows the fitting curve for lifetime changes with increased concentration of  $\text{Ni}^{2+}/\text{H}_2\text{A}$ . Conditions: pH of all solutions was adjusted to 4.5; excitation wavelength: 406 nm

for photocatalysis<sup>59</sup>, and exceptional hydrogen evolution efficiency was achieved based on CdSe/CdS QDs with  $\text{S}^{2-}$  ligands<sup>32</sup>. So here we attribute the superior hydrogen evolution efficiency with InP/ZnS-S QDs to the replacement of conventional organic ligands by inorganic sulfide ligands.

Transient photocurrent measurements (Fig. 5b) show that InP/ZnS-OLA QDs barely respond to light. In contrast, InP/ZnS-MPA QDs and InP/ZnS-S QDs displayed a quick light response. Especially InP/ZnS-S QDs exhibited a higher current density than InP/ZnS-MPA QDs, i.e., InP/ZnS-S QDs exhibit favorable interaction with their reaction system. Additionally, electrochemical impedance spectroscopy (EIS) data show that FTO electrodes covered with InP/ZnS-S QDs exhibit the lowest resistance under light illumination among the test series (Fig. 5c). Fitting results indicated that  $R_{\text{ct}}$  was  $2.3 \times 10^4$ ,  $7.8 \times 10^4$ ,  $1.4 \times 10^6$ , and  $6.2 \times 10^5 \Omega$  for FTO covered with InP/ZnS-S, -MPA, -OLA QDs and blank FTO, respectively (see Supplementary Fig. 22 and Supplementary Table 8). Note that the  $R_{\text{ct}}$  of InP/ZnS-OLA QDs even exceeds the blank value, thereby indicating that organic ligands inhibit charge transportation. Alternatively, InP/ZnS-S QDs may display more active interfaces compared to InP/ZnS-MPA QDs. Compared to organic ligands, such as OLA and MPA, the single anion  $\text{S}^{2-}$  can far more easily circumvent the physical and electrical barriers arising from the large volume and insulator carbon chains of organic ligands<sup>58,60,61</sup>. This may facilitate the migration of charge carriers from the QDs towards other components of the reaction systems, in particular  $\text{H}_2\text{A}$  or  $\text{Ni}^{2+}$ . Additionally, this may be the reason why InP/ZnS-MPA QDs are much better photosensitizers than InP/ZnS-MUA QDs, given that the carbon chain of MPA (3) is shorter than that of MUA (11).

After confirming the superior activity of sulfide ligands over organic thiol ligands in the present system for hydrogen

evolution, we furthermore synthesized InP/ZnS QDs capped with  $\text{Cl}^-$  and  $\text{PO}_4^{3-}$  (denoted as InP/ZnS-Cl and InP/ZnS- $\text{PO}_4$  QDs, details in Supplementary Method 8) to explore possible differences between InP/ZnS-S QDs and those with other inorganic ligands. Interestingly, the hydrogen evolution efficiency in the presence of these QDs was also much lower than that of InP/ZnS-S QDs (Fig. 5d and Supplementary Fig. 23 for InP QDs). In combination with the above results, we tentatively attribute this to the effective hole transfer from the intrinsic QDs to sulfide, which is more difficult for chloride and phosphide due to their relatively positive oxidation potential.

Electron paramagnetic resonance (EPR) spectroscopy was then performed to obtain further information on the different all-inorganic QD types. As shown in Fig. 5e and Supplementary Fig. 24, no obvious signals could be observed for all QDs in the dark. With light on, still no obvious signal was recorded for InP/ZnS-Cl and - $\text{PO}_4$  QDs. However, for InP/ZnS-S QDs, a signal around a  $g$  factor of 2.006 immediately emerges after light irradiation. The absence of this signal in the dark indicates that it is highly related to the photogenerated exciton, rather than to the intrinsic structure defects or surface states of the QDs<sup>62</sup>. Careful examination further shows that it does not arise from photogenerated holes in InP QDs ( $g = 2.001$ )<sup>62,63</sup>. Instead, it is probably due to electrons in the conduction bands of InP QDs ( $g = 2.006$ ) according to the relevant literature<sup>62,63</sup>. This hypothesis was further confirmed by control experiments: after the introduction of  $\text{H}_2\text{A}$  into the system to deplete the photogenerated holes, this signal became much more evident (Supplementary Fig. 24). As all the QDs in our test are derivatives of InP/ZnS-OLA QDs, their interior exciton processes should be similar. We therefore believe that this electron related signal in our system is directly related to the hole capture ability of the surface ligands.

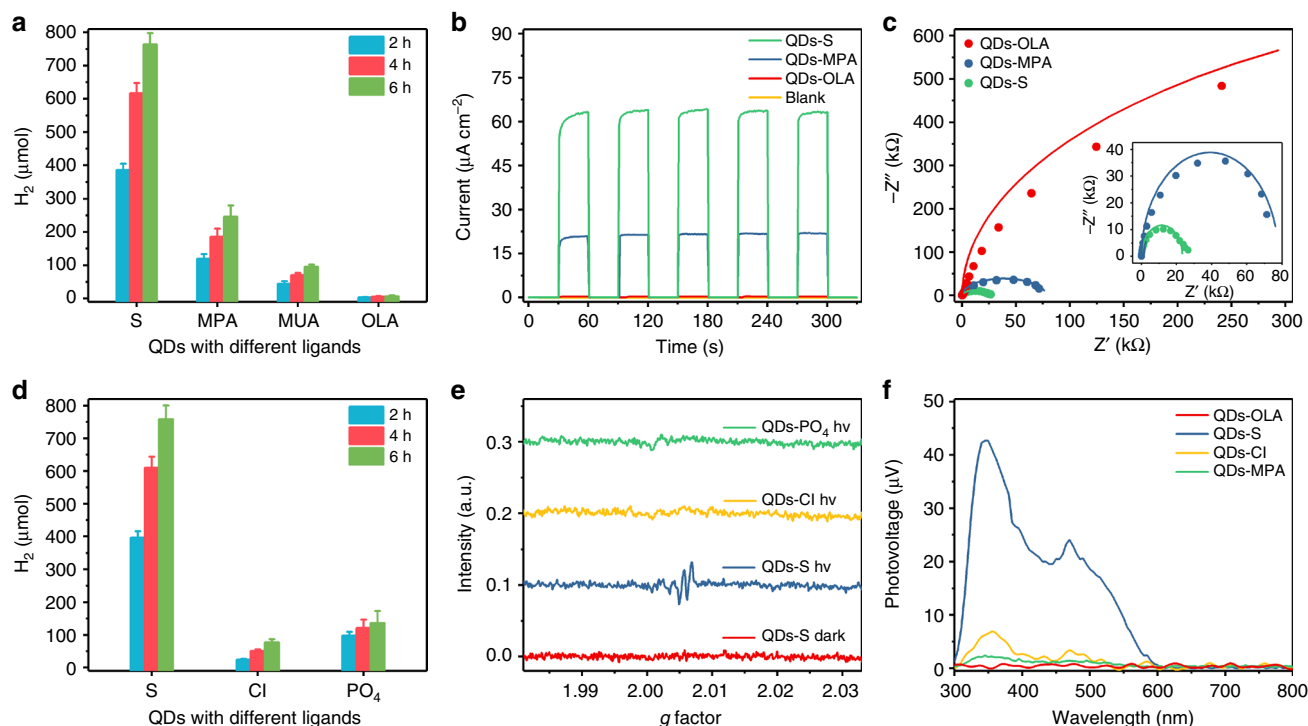


**Fig. 5** Influence of different ligands on the hydrogen evolution performance and photophysical properties of InP/ZnS QDs (525 nm, 15 min). **a** Hydrogen evolution for InP/ZnS QDs capped with different organic ligands. Conditions: 1.6  $\mu\text{M}$  QDs and 0.035 mM  $\text{Ni}^{2+}$  in 6 mL of 0.2 M  $\text{H}_2\text{A}$  (pH 4.5) were illuminated with a LED light source (525 nm,  $4 \times 1 \text{ W}$ ). **b** Transient photocurrent and **c** electrochemical impedance spectra of InP/ZnS QDs with different ligands at open circuit voltage under simulated sunlight illumination. Conditions: electrolyte: 0.2 M  $\text{H}_2\text{A}$ , pH 4.5; frequency range: 0.1– $10^5$  Hz. **d** Hydrogen evolution for InP/ZnS QDs capped with different inorganic ligands. Conditions: 1.6  $\mu\text{M}$  QDs and 0.035 mM  $\text{Ni}^{2+}$  in 6 mL of 0.2 M  $\text{H}_2\text{A}$  (pH 4.5) were illuminated with a LED light source (525 nm,  $4 \times 1 \text{ W}$ ). **e** EPR spectra for InP/ZnS QDs with different ligands. The magnetic field intensity was transformed into  $g$  factor values. **f** SPV spectra for InP/ZnS QDs capped with different ligands. Xe lamp was used for irradiation. Error bars were estimated based on the standard deviation according to three independent experiments

Accordingly, we conclude that holes in InP/ZnS-S QDs effectively transfer from the interior to surface  $\text{S}^{2-}$ , which in return significantly increases the stability of electrons in the conducting band and renders them detectable in the EPR spectra at room temperature. As a contrast, the hole transfer from QDs to  $\text{Cl}^-$  or  $\text{PO}_4^{3-}$  is limited and the relevant signals are not obvious (Fig. 5e).

Moreover, surface photovoltage spectra (SPV) of InP/ZnS-S, -OLA, -MPA, and -Cl QDs were recorded to obtain more information about different charge separation and transportation characteristics of  $\text{S}^{2-}$  capped QDs compared to those equipped with other typical organic and inorganic ligands. No photovoltage existed beyond 600 nm for QDs, and this is in accordance with the absorption spectrum of QDs, meaning that no sub-band gap excitation from the trapped state contributes to the photogenerated charge transfer process<sup>64</sup>. The corresponding photovoltage generated by -S QDs is obviously much larger than that of -OLA, -Cl, and -MPA QDs (Fig. 5f), confirming the efficient charge separation of the sulfide capped particles once again<sup>65</sup>. The positive response means that positive charge accumulated at the interface under irradiation<sup>66</sup>, further demonstrating that sulfide ligands extract holes to the surface of InP/ZnS-S QDs, in line with the above TA and EPR experiments. Besides, strong interdot coupling and band-like charge transport may exist in QDs capped with inorganic ligands, such as  $\text{S}^{2-}$  or  $\text{Cl}^-$ <sup>30,67</sup>, which could contribute to their higher charge mobility and resulting higher photovoltage in contrast to MPA and OLA capped QDs.

Furthermore, density functional theory (DFT) calculations (Supplementary Method 1, Supplementary Figs. 25–27, and Supplementary Note 3) also indicate that introduction of S centers on the surface of the QDs is beneficial for charge transfer,

which is consistent with the above experiments and analyses. Moreover, the nature of  $\text{S}^{2-}$  ligands is different from the intrinsic defects on InP QDs, and the latter can be suppressed by the introduction of ZnS.

## Discussion

As the surface  $\text{S}^{2-}$  ligands may be regarded as a kind of surface trap, which is indicated by the decrease of the QD luminescence, we further analyze the different role of  $\text{S}^{2-}$  ligands compared to the ordinary intrinsic defects of QDs according to the above experimental measurements and theoretical calculations (Supplementary Fig. 28). The ordinary intrinsic defects on QDs are often disordered, and they always act as recombination centers for holes and electrons, which both lowers the band-edge emission of QDs and reduces the charge separation efficiency<sup>68</sup>. In our work, the introduction of ZnS on InP QDs can be considered as a suitable strategy to decrease the amount of intrinsic defects which are detrimental for photocatalysis with QDs. The effectiveness of this approach is proven by the higher PLQY and hydrogen evolution efficiency after ZnS layer growth. Alternatively, the introduction of  $\text{S}^{2-}$  ligands can be regarded as an exterior trap<sup>69</sup>. Although the surface  $\text{S}^{2-}$  ligands decrease the emission of QDs in the present case, they improve the charge separation efficiency of the system because of their hole capture ability. That is, after light excitation of QDs, the holes can transfer quickly to the  $\text{S}^{2-}$  ligands, which is beneficial for electron/hole separation. Moreover, the small volume of  $\text{S}^{2-}$  in comparison to the traditional organic ligands lowers the barrier for further hole transfer from  $\text{S}^{2-}$  to  $\text{H}_2\text{A}$ .

In summary, we have successfully introduced inorganic  $S^{2-}$ -capped InP and InP/ZnS QDs as efficient photosensitizers for hydrogen evolution. InP/ZnS QDs reach TON values up to 128,000 per QDs and an internal quantum yield of 31% (525 nm). This demonstrates the remarkable potential of  $S^{2-}$ -capped InP-based QDs for photocatalytic applications. Moreover, using a series of spectroscopic and photoelectrochemical characterizations, we demonstrate that inorganic sulfide ligands on QDs are beneficial for the photocatalytic hydrogen evolution. In comparison with conventional organic ligands and other inorganic ligands, sulfide ions on the surface can extract the holes from the interior of QDs rapidly, followed by their reaction with  $H_2A$  via low physical and electronic barriers. This leads to efficient charge separation and notably enhances the photocatalytic hydrogen evolution performance. Key perspectives for further progress are the development of other InP-based heterostructures, and the application of inorganic sulfide capped InP QDs for a wider spectrum of photocatalytic reactions.

## Methods

**Synthesis of 525 nm InP and InP/ZnS QDs.** In total 111 mg (0.5 mmol) of indium(III) chloride as indium precursor, 204 mg (1.5 mmol) of zinc(II) chloride and 160 mg (0.5 mmol) zinc(II) iodide as zinc precursors were mixed in 5.0 mL (15 mmol) of oleylamine. Here Zn precursors were added to assist in controlling the size distribution of InP QDs<sup>28</sup>. The reaction mixture was then evacuated by Schlenk techniques and kept under vacuum at 120 °C for 1 h. Afterwards, the system was heated to 180 °C under inert atmosphere. 0.5 mL (1.8 mmol) of tris (diethylamino)phosphine (phosphorous: indium ratio = 3.6: 1) was then quickly injected into the mixture. The system was kept at 180 °C for 30 min to drive the growth of InP QDs to completion and then cooled to room temperature.

For InP/ZnS QDs, after the above system was kept at 180 °C for 30 min, it was further heated to 260 °C instead of cooling down, and 1 mL of trioctylphosphine (TOP)-S (2 M) solution was slowly added with a rate of 0.2 mL min<sup>-1</sup> (TOP-S solution was made by dissolving 0.128 g of sulfur in 2 mL of TOP by heating or ultrasound under inert atmosphere). Time measurement for ZnS layer growth was started after the whole TOP-S solution had been added, and the reaction was stopped after different times. Finally, the system was cooled down to room temperature.

After the above crude QD solution was cooled down to room temperature, about 10 mL of ethanol (EtOH) were added for the precipitation of QDs. After centrifugation, the supernatant was discarded. The precipitated QDs were further purified by dissolution in 10 mL of hexane (HEX) and subsequent precipitation in 15 mL of ethanol. Finally, the QDs were again dissolved in 20 mL of HEX and centrifuged to remove the insoluble impurities. The prepared QDs could be well kept in solution at 2–6 °C.

**Synthesis of QDs with different excitonic absorption peaks.** To synthesize InP and InP/ZnS QDs with excitonic absorption peaks located at other wavelengths, different ratios of zinc(II) chloride and zinc(II) iodide precursors were added. The remaining processes were performed as described above. In summary: when 2 mmol of zinc(II) chloride was used, QDs with an absorption peak around 570 nm were obtained; when 1 mmol of zinc(II) chloride and 1 mmol of zinc(II) iodide were used, QDs with an absorption peak around 480 nm were obtained; when 0.5 mmol of zinc(II) chloride and 1.5 mmol of zinc(II) iodide were used, QDs with an absorption peak around 435 nm were obtained. For QDs with short absorption peak, the purification process is somewhat more demanding (see Supplementary Note 1). For the sake of clarity, we refer to InP QDs with excitonic absorption peak at X nm as InP QDs (X nm) and to InP/ZnS with ZnS growth time of Y min as InP/ZnS QDs (Y min).

**$S^{2-}$  ligand exchange for InP and InP/ZnS QDs.** Solutions for ligand exchange with  $S^{2-}$  were prepared by dissolving  $Na_2S \cdot 9H_2O$  in highly polar solvents, namely formamide (FA) or N-methylformamide (NMF). Ligand exchange with  $S^{2-}$  can be carried out directly under ambient conditions and usually proceeded within 5 min to 1 h, depending on the kind of polar solvent, concentrations of QDs and  $S^{2-}$ , stirring speed and temperature. No obvious difference was observed when the ligand exchange was performed in air or under inert atmosphere. In a typical process, 1 mL of InP or InP/ZnS QDs (about 3–5 mg mL<sup>-1</sup>) in HEX were mixed with 1 mL of  $Na_2S \cdot 9H_2O$  (0.05 M) solution dissolved in NMF. The mixture was kept stirring at room temperature until a total phase transfer for QDs from HEX to NMF was achieved. This transfer process can be easily monitored by the color change of the HEX (red to colorless) and NMF (colorless to red) phases. The HEX phase was then discarded and the NMF phase was further washed with HEX twice to remove any remaining nonpolar organic species. The washed NMF phase was precipitated with 3 mL acetone and purified with 0.5 mL FA and 1 mL acetone.

Finally, the precipitate was redissolved in water by ultrasound. Afterwards, the solution was centrifuged to remove any insoluble QDs and impurities, and the obtained colloidal aqueous solution of QDs was stored at 2–6 °C.

**Photocatalytic hydrogen evolution tests.** Typical hydrogen evolution experiments were performed with 6 mL of  $H_2O$  solution containing 1.6  $\mu M$  QDs, 0.035 mM  $NiCl_2 \cdot 6H_2O$ , and 0.2 M  $H_2A/NaHA$  in a Pyrex tube at pH 4.5. The pH of the mixed solution can be easily adjusted by changing the ratio of  $H_2A$  to  $NaHA$ . After deoxygenation with argon for 20 min, the system was irradiated with a home-made LED reactor with 4 pcs of 525 nm bulbs (Tao Yuan, China; 4 × 1 W) under constant stirring and circular water cooling. Other light sources such as 4 pcs of 465 nm LED (Tao Yuan, China; 4 × 1 W) and AM 1.5 simulator (LOT-Oriel, LS0306) were also used in the photocatalytic experiments. The photogenerated  $H_2$  was quantified by GC (Varian CP-3800) using argon as the carrier gas with a molecular sieve column (5 Å) and a thermal conductivity detector. To ensure reproducibility, two or more independent measurements were performed. As a data treatment, the standard deviation (showed as error bar) was increased to 5% of the average value if it was below this threshold<sup>15</sup>.

In addition, we also used an on-line hydrogen evolution and detection system developed in house. The system was irradiated by one LED bulb with 453 nm wavelength of tunable intensity. Gas chromatograms were recorded using an automated Bruker GC 456 gas chromatograph with argon as the carrier gas and a 3 m × 2 mm packed molecular sieve 13 × 80–100 column. The column and reference gas flow (Ar) were set to 20 mL min<sup>-1</sup>. The oven was operated isothermally at 100 °C. An argon flow of 6 mL min<sup>-1</sup> (adjusted with an onboard EFC device and referenced with a F-200CV-002 from Bronkhorst) was passed through the reaction mixture and into the GC, where 1 mL gas samples were automatically injected in defined time intervals (5 min) using a 6-Port-2-position Valve from Vici. The gases were detected using a thermal conductivity detector operated at 150 °C (retention time is about 1 min for  $H_2$ ). Data were then analyzed with the software Origin Pro.

## Data availability

The data that support the findings of this study are available from the corresponding authors upon request.

Received: 22 February 2018 Accepted: 28 August 2018

Published online: 01 October 2018

## References

1. Chu, S., Cui, Y. & Liu, N. The path towards sustainable energy. *Nat. Mater.* **16**, 16–22 (2017).
2. Mao, S. S. & Shen, S. Hydrogen production: catalysing artificial photosynthesis. *Nat. Photonics* **7**, 944–946 (2013).
3. Zhang, G., Lan, Z.-A. & Wang, X. Conjugated polymers: catalysts for photocatalytic hydrogen evolution. *Angew. Chem. Int. Ed.* **55**, 15712–15727 (2016).
4. Moniz, S. J. A., Shevlin, S. A., Martin, D. J., Guo, Z.-X. & Tang, J. Visible-light driven heterojunction photocatalysts for water splitting – a critical review. *Energy Environ. Sci.* **8**, 731–759 (2015).
5. Kudo, A. & Miseki, Y. Heterogeneous photocatalyst materials for water splitting. *Chem. Soc. Rev.* **38**, 253–278 (2009).
6. Esswein, A. J. & Nocera, D. G. Hydrogen production by molecular photocatalysis. *Chem. Rev.* **107**, 4022–4047 (2007).
7. Weingarten, A. S. et al. Supramolecular packing controls  $H_2$  photocatalysis in chromophore amphiphile hydrogels. *J. Am. Chem. Soc.* **137**, 15241–15246 (2015).
8. Khnayzer, R. S., McCusker, C. E., Olaiya, B. S. & Castellano, F. N. Robust cuprous phenanthroline sensitizer for solar hydrogen photocatalysis. *J. Am. Chem. Soc.* **135**, 14068–14070 (2013).
9. Talapin, D. V., Lee, J.-S., Kovalenko, M. V. & Shevchenko, E. V. Prospects of colloidal nanocrystals for electronic and optoelectronic applications. *Chem. Rev.* **110**, 389–458 (2010).
10. Wu, K. & Lian, T. Quantum confined colloidal nanorod heterostructures for solar-to-fuel conversion. *Chem. Soc. Rev.* **45**, 3781–3810 (2016).
11. Harris, R. D. et al. Electronic processes within quantum dot-molecule complexes. *Chem. Rev.* **116**, 12865–12919 (2016).
12. Han, Z. & Eisenberg, R. Fuel from water. The photochemical generation of hydrogen from water. *Acc. Chem. Res.* **47**, 2537–2544 (2014).
13. Wu, L.-Z., Chen, B., Li, Z.-J. & Tung, C.-H. Enhancement of the efficiency of photocatalytic reduction of protons to hydrogen via molecular assembly. *Acc. Chem. Res.* **47**, 2177–2185 (2014).
14. Fang, Y. et al. Intermittent photocatalytic activity of single CdS nanoparticles. *Proc. Natl Acad. Sci. USA* **114**, 10566–10571 (2017).
15. Wakerley, D. W. et al. Solar-driven reforming of lignocellulose to  $H_2$  with a CdS/CdO<sub>x</sub> photocatalyst. *Nat. Energy* **2**, 17021 (2017).



16. Holmes, M. A., Townsend, T. K. & Osterloh, F. E. Quantum confinement controlled photocatalytic water splitting by suspended CdSe nanocrystals. *Chem. Commun.* **48**, 371–373 (2012).
17. Han, Z., Qiu, F., Eisenberg, R., Holland, P. L. & Krauss, T. D. Robust photogeneration of H<sub>2</sub> in water using semiconductor nanocrystals and a nickel catalyst. *Science* **338**, 1321–1324 (2012).
18. Kalisman, P., Nakibli, Y. & Amirav, L. Perfect photon-to-hydrogen conversion efficiency. *Nano. Lett.* **16**, 1776–1781 (2016).
19. Yu, S. et al. Vectorial electron transfer for improved hydrogen evolution by mercaptopropionic-acid-regulated CdSe quantum-dots-TiO<sub>2</sub>-Ni(OH)<sub>2</sub> assembly. *ChemSusChem* **8**, 642–649 (2015).
20. Jian, J.-X. et al. Chitosan confinement enhances hydrogen photogeneration from a mimic of the diiron subsite of [FeFe]-hydrogenase. *Nat. Commun.* **4**, 2695 (2013).
21. Li, Q., Li, X., Wageh, S., Al-Ghamdi, A. A. & Yu, J. CdS/Graphene nanocomposite photocatalysts. *Adv. Energy Mater.* **5**, 1500010 (2015).
22. Courtney, C. M. et al. Photoexcited quantum dots for killing multidrug-resistant bacteria. *Nat. Mater.* **15**, 529–534 (2016).
23. Regulacio, M. D. & Han, M.-Y. Multinary I-III-VI<sub>2</sub> and I<sub>2</sub>-II-IV-VI<sub>4</sub> semiconductor nanostructures for photocatalytic applications. *Acc. Chem. Res.* **49**, 511–519 (2016).
24. Fan, G., Wang, C. & Fang, J. Solution-based synthesis of III–V quantum dots and their applications in gas sensing and bio-imaging. *Nano Today* **9**, 69–84 (2014).
25. Brunetti, V. et al. InP/ZnS as a safer alternative to CdSe/ZnS core/shell quantum dots: in vitro and in vivo toxicity assessment. *Nanoscale* **5**, 307–317 (2013).
26. Nann, T. et al. Water splitting by visible light: a nanophotocathode for hydrogen production. *Angew. Chem. Int. Ed.* **49**, 1574–1577 (2010).
27. Wallentin, J. et al. InP nanowire array solar cells achieving 13.8% efficiency by exceeding the ray optics limit. *Science* **339**, 1057 (2013).
28. Tessier, M. D., Dupont, D., Nolf, K., de Roo, de, J. & Hens, Z. Economic and size-tunable synthesis of InP/ZnE (E=S, Se) colloidal quantum dots. *Chem. Mater.* **27**, 4893–4898 (2015).
29. Kovalenko, M. V., Scheele, M. & Talapin, D. V. Colloidal nanocrystals with molecular metal chalcogenide surface ligands. *Science* **324**, 1417–1420 (2009).
30. Nag, A. et al. Metal-free inorganic ligands for colloidal nanocrystals: S<sup>2-</sup>, HS<sup>-</sup>, Se<sup>2-</sup>, HSe<sup>-</sup>, Te<sup>2-</sup>, HTe<sup>-</sup>, OH<sup>-</sup>, and NH<sub>2</sub><sup>-</sup> as surface ligands. *J. Am. Chem. Soc.* **133**, 10612–10620 (2011).
31. Wang, R. et al. Colloidal quantum dot ligand engineering for high performance solar cells. *Energy Environ. Sci.* **9**, 1130–1143 (2016).
32. Li, Z.-J. et al. Direct synthesis of all-inorganic heterostructured CdSe/CdS QDs in aqueous solution for improved photocatalytic hydrogen generation. *J. Mater. Chem. A* **5**, 10365–10373 (2017).
33. Tessier, M. D. et al. Aminophosphines. A double role in the synthesis of colloidal indium phosphide quantum dots. *J. Am. Chem. Soc.* **138**, 5923–5929 (2016).
34. Xie, R., Battaglia, D. & Peng, X. Colloidal InP nanocrystals as efficient emitters covering blue to near-infrared. *J. Am. Chem. Soc.* **129**, 15432–15433 (2007).
35. Li, L. & Reiss, P. One-pot synthesis of highly luminescent InP/ZnS nanocrystals without precursor injection. *J. Am. Chem. Soc.* **130**, 11588–11589 (2008).
36. Tamang, S., Lincheneau, C., Hermans, Y., Jeong, S. & Reiss, P. Chemistry of InP nanocrystal syntheses. *Chem. Mater.* **28**, 2491–2506 (2016).
37. Zhang, H. et al. Surfactant ligand removal and rational fabrication of inorganically connected quantum dots. *Nano. Lett.* **11**, 5356–5361 (2011).
38. Pu, C. & Peng, X. To battle surface traps on CdSe/CdS core/shell nanocrystals: shell isolation versus surface treatment. *J. Am. Chem. Soc.* **138**, 8134–8142 (2016).
39. Wei, H. H.-Y. et al. Colloidal semiconductor quantum dots with tunable surface composition. *Nano. Lett.* **12**, 4465–4471 (2012).
40. Xi, L. et al. Understanding the role of single molecular ZnS precursors in the synthesis of In(Zn)P/ZnS nanocrystals. *ACS Appl. Mater. Interfaces* **6**, 18233–18242 (2014).
41. Li, Z. J. et al. Visible light catalysis-assisted assembly of Ni<sub>0</sub>-QD hollow nanospheres in situ via hydrogen bubbles. *J. Am. Chem. Soc.* **136**, 8261–8268 (2014).
42. Zhu, H., Song, N. & Lian, T. Controlling charge separation and recombination rates in CdSe/ZnS Type I core–shell quantum dots by shell thicknesses. *J. Am. Chem. Soc.* **132**, 15038–15045 (2010).
43. Martindale, B. M. C., Joliat, E., Bachmann, C., Alberto, R. & Reisner, E. Clean donor oxidation enhances the H<sub>2</sub> evolution activity of a carbon quantum dot–molecular catalyst photosystem. *Angew. Chem. Int. Ed.* **55**, 9402–9406 (2016).
44. Liu, J., Yang, W., Li, Y., Fan, L. & Li, Y. Electrochemical studies of the effects of the size, ligand and composition on the band structures of CdSe, CdTe and their alloy nanocrystals. *Phys. Chem. Chem. Phys.* **16**, 4778–4788 (2014).
45. Gimbert-Suriñach, C. et al. Efficient and limiting reactions in aqueous light-induced hydrogen evolution systems using molecular catalysts and quantum dots. *J. Am. Chem. Soc.* **136**, 7655–7661 (2014).
46. Ye, Y. et al. Charge-transfer dynamics promoted by hole trap states in CdSe quantum dots–Ni<sup>2+</sup> photocatalytic system. *J. Phys. Chem. C* **121**, 17112–17120 (2017).
47. Wang, X. et al. Odd–even effect of thiophene chain lengths on excited state properties in Oligo(thienyl ethynylene)-cored chromophores. *J. Phys. Chem. C* **121**, 7659–7666 (2017).
48. Klimov, V. I. Optical nonlinearities and ultrafast carrier dynamics in semiconductor nanocrystals. *J. Phys. Chem. B* **104**, 6112–6123 (2000).
49. Wu, K., Zhu, H., Liu, Z., Rodríguez-Córdoba, W. & Lian, T. Ultrafast charge separation and long-lived charge separated state in photocatalytic CdS–Pt nanorod heterostructures. *J. Am. Chem. Soc.* **134**, 10337–10340 (2012).
50. Wu, K. et al. Interfacial charge separation and recombination in InP and quasi-type II InP/CdS core/shell quantum dot–molecular acceptor complexes. *J. Phys. Chem. A* **117**, 7561–7570 (2013).
51. McArthur, E. A., Morris-Cohen, A. J., Knowles, K. E. & Weiss, E. A. Charge carrier resolved relaxation of the first excitonic state in CdSe quantum dots probed with near-infrared transient absorption spectroscopy. *J. Phys. Chem. B* **114**, 14514–14520 (2010).
52. Zeng, Y. & Kelley, D. F. Excited hole photochemistry of CdSe/CdS quantum dots. *J. Phys. Chem. C* **120**, 17853–17862 (2016).
53. Blackburn, J. L. et al. Electron and hole transfer from indium phosphide quantum dots. *J. Phys. Chem. B* **109**, 2625–2631 (2005).
54. Tseng, H.-W., Wilker, M. B., Damrauer, N. H. & Dukovic, G. Charge transfer dynamics between photoexcited CdS nanorods and mononuclear Ru water-oxidation catalysts. *J. Am. Chem. Soc.* **135**, 3383–3386 (2013).
55. Schnitzenbaumer, K. J., Labrador, T. & Dukovic, G. Impact of chalcogenide ligands on excited state dynamics in CdSe quantum dots. *J. Phys. Chem. C* **119**, 13314–13324 (2015).
56. Lian, S., Kodaimati, M. S., Dolzhenkov, D. S., Calzada, R. & Weiss, E. A. Powering a CO<sub>2</sub> reduction catalyst with visible light through multiple sub-picosecond electron transfers from a quantum dot. *J. Am. Chem. Soc.* **139**, 8931–8938 (2017).
57. Hetsch, F., Zhao, N., Kershaw, S. V. & Rogach, A. L. Quantum dot field effect transistors. *Mater. Today* **16**, 312–325 (2013).
58. Yun, H. J., Paik, T., Edley, M. E., Baxter, J. B. & Murray, C. B. Enhanced charge transfer kinetics of CdSe quantum dot-sensitized solar cell by inorganic ligand exchange treatments. *ACS Appl. Mater. Interfaces* **6**, 3721–3728 (2014).
59. Chang, C. M., Orchard, K. L., Martindale, B. C. M. & Reisner, E. Ligand removal from CdS quantum dots for enhanced photocatalytic H<sub>2</sub> generation in pH neutral water. *J. Mater. Chem. A* **4**, 2856–2862 (2016).
60. Nag, A. et al. Effect of metal ions on photoluminescence, charge transport, magnetic and catalytic properties of all-inorganic colloidal nanocrystals and nanocrystal solids. *J. Am. Chem. Soc.* **134**, 13604–13615 (2012).
61. Schnitzenbaumer, K. J. & Dukovic, G. Chalcogenide-ligand passivated CdTe quantum dots can be treated as core/shell semiconductor nanostructures. *J. Phys. Chem. C* **118**, 28170–28178 (2014).
62. Micić, O. I. et al. Electron and hole adducts formed in illuminated inorganic colloidal quantum dots studied by electron paramagnetic resonance. *J. Phys. Chem. B* **106**, 4390–4395 (2002).
63. Dimitrijević, N. M. et al. Charge separation in heterostructures of InP nanocrystals with metal particles. *J. Phys. Chem. B* **109**, 18243–18249 (2005).
64. Kronik, L. & Shapira, Y. Surface photovoltage spectroscopy of semiconductor structures: at the crossroads of physics, chemistry and electrical engineering. *Surf. Interface Anal.* **31**, 954–965 (2001).
65. Jiao, X. et al. Defect-mediated electron-hole separation in one-unit-cell ZnIn<sub>2</sub>S<sub>4</sub> layers for boosted solar-driven CO<sub>2</sub> reduction. *J. Am. Chem. Soc.* **139**, 7586–7594 (2017).
66. Zhao, J., Nail, B. A., Holmes, M. A. & Osterloh, F. E. Use of surface photovoltage spectroscopy to measure built-in voltage, space charge layer width, and effective band gap in CdSe quantum dot films. *J. Phys. Chem. Lett.* **7**, 3335–3340 (2016).
67. Choi, J.-H. et al. Bandlike transport in strongly coupled and doped quantum dot solids. A route to high-performance thin-film electronics. *Nano. Lett.* **12**, 2631–2638 (2012).
68. Liu, X.-Y. et al. 0D–2D quantum dot: metal dichalcogenide nanocomposite photocatalyst achieves efficient hydrogen generation. *Adv. Mater.* **29**, 1605646 (2017).
69. Xie, Y.-P., Yu, Z. B., Liu, G., Ma, X. L. & Cheng, H.-M. CdS–mesoporous ZnS core–shell particles for efficient and stable photocatalytic hydrogen evolution under visible light. *Energy Environ. Sci.* **7**, 1895–1901 (2014).

## Acknowledgements

We are grateful for financial support from the Sino Swiss Science and Technology Corporation (SSSTC project EG 08-032015), from the Sichuan Provincial International

Cooperation Project (2017HH0030), from the Innovative Research Team of Sichuan Province (2016TD0011) and from the starting project of SWPU (No. 2015QHZ018). This work has been supported by the University of Zurich Research Priority Program “Solar Light to Chemical Energy Conversion” (URPP LightChEC) and by the Swiss National Science Foundation (Sinergia Grant No. CRSII2\_160801/1). We thank Dr. Benjamin Probst and Prof. Dr. Roger Alberto (Department of Chemistry, University of Zurich) for support with online hydrogen evolution tests, and Beijing China Education Au-light Co.,Ltd for providing the instrument and assistance with SPV measurements.

### Author contributions

G.R.P., Y.Z. and L.-Z.W. conceived the research. S.Y. and X.-B.F. designed the experiments and performed the synthesis, characterization and photocatalysis. X.W. and A.X. performed the femtosecond transient absorption measurement. J.L. and Q.Z. performed the electrochemistry and the photoelectric measurements. S.W. performed the DFT calculations. S.Y., X.-B.F. and G.R.P. wrote the manuscript. All authors analyzed the data and commented on the manuscript.

### Additional information

**Supplementary Information** accompanies this paper at <https://doi.org/10.1038/s41467-018-06294-y>.

**Competing interests:** The authors declare no competing interests.

**Reprints and permission** information is available online at <http://npg.nature.com/reprintsandpermissions/>

**Publisher's note:** Springer Nature remains neutral with regard to jurisdictional claims in published maps and institutional affiliations.



**Open Access** This article is licensed under a Creative Commons Attribution 4.0 International License, which permits use, sharing, adaptation, distribution and reproduction in any medium or format, as long as you give appropriate credit to the original author(s) and the source, provide a link to the Creative Commons license, and indicate if changes were made. The images or other third party material in this article are included in the article's Creative Commons license, unless indicated otherwise in a credit line to the material. If material is not included in the article's Creative Commons license and your intended use is not permitted by statutory regulation or exceeds the permitted use, you will need to obtain permission directly from the copyright holder. To view a copy of this license, visit <http://creativecommons.org/licenses/by/4.0/>.

© The Author(s) 2018